J Vis (2023) 26:83–96
https://doi.org/10.1007/s12650-022-00866-3

REGULAR PAPER

Jayabal Rajasekar · Minoru Yaga · Heuy Dong Kim

Numerical prediction on the mitigation of shock wave using geometric barriers

Received: 7 October 2020 / Revised: 11 July 2022 / Accepted: 12 July 2022 / Published online: 30 July 2022

Abstract The propagation and mitigation of shock waves inside the shock tube have a great interest to researchers. This study focuses on shock wave mitigation using different geometric barriers inside the shock tube's driven section. The underlying concept of shock mitigation is to produce a multiple reflection and diffraction of a shock wave with very minimum flow obstructions. The planar shock wave generated from the shock tube interacted with different geometric barriers like a zig-zag barrier, inclined barrier, and staggered vertical barrier was studied computationally and discussed. In the zig-zag barrier case, the shock wave was repeatedly reflected and diffracted inside the geometrical passage without any obstructions and mitigated the shock wave. On the other hand, inclined and staggered vertical barrier cases involve the alternate flow obstruction due to the barrier, which retards the mass motion velocity. It results in a significant reduction of shock pressure in the downstream region. The numerical analysis was simulated using the inviscid and Navier–Stokes equations with air as an ideal gas. The numerical model was validated based on the experimental results. The numerical studies show that the geometric barriers have a considerable impact on the mitigation of shock wave inside the shock tube.

Keywords Shock mitigation · Shock tube · Unsteady flow · Reflection · Diffraction · Compressible flow

1 Introduction

In recent decades, fluid–structure interaction has been the interest of numerous computational researchers. This paper deals with the fundamental physics involved in the shock tube and mitigation of shock wave due to the employment of geometrical barriers. In the shock tube, after the diaphragm rupture, the planar shock wave develops and propagates in the uniform cross-section duct (Needham 2018). The shock wave attenuates because of the strong dissipative actions inherently implicit in the shock wave itself. The geometric barrier with a very minimal obstruction area is employed in the duct's driven section to mitigate the shock wave instantly. The critical mechanism responsible for the mitigation of shock wave is diffraction and reflection initiated due to the expansion and compression of shock waves. The multiple reflection and diffraction phenomenon inside the shock tube results in the mitigation of shock strength in the downstream region. As per the shock wave theory, the reflected shock wave has a higher shock magnitude than the incident shock wave (Rajasekar et al. 2020). Hence, more interest goes towards mitigation of shock magnitude and shock impulse before it hits the target.

J. Rajasekar · H. D. Kim (✉)
Department of Mechanical Engineering, Andong National University, Andong, Korea
E-mail: kimhd@anu.ac.kr

M. Yaga
Faculty of Engineering, University of the Ryukyus, 1 Senbaru, Nishihara, Okinawa 903-0213, Japan

The literature survey shows that the most prominent mitigation strategy is to implement geometric blockage like baffle plates, orifice plate, grids, perforated plate, set of solid obstacles of different shapes were previously investigated (Ohtomo et al. 2005; Britan et al. 2006; Berger et al. 2010; Chaudhuri et al. 2013). These geometrical blockages lead to shock wave reflections and shock wave diffractions, which can considerably mitigate the shock wave. The peak overpressure behind the shock wave was reduced. Igra et al. designed a bend in a shock tube and implemented the surface roughness to mitigate the shock wave inside the duct to improve the results (Igra et al. 2001). In some studies, shock-absorbing materials were used to reduce shock pressure at target locations. Material like porous compressible foam is used as absorbing material. It undergoes plastic deformation and absorbs the shock significantly (Baer 1992; Britan et al. 2013; Petel et al. 2013). Sommerfeld studied the presence of a tiny solid object or liquid droplet in the gaseous flow makes a considerable impact on shock strength (Sommerfeld 1985). Bakken et al. studied the attenuation effects due to granular filters (Bakken et al. 2003). Sembian investigated the implementation of aqueous foam barriers that significantly impacted shock strength reduction (Sembian et al. 2016). Few studies involve polymer foams like polyurethane or polystyrene as shock absorbers during impact loading (Sounik et al. 1997; Song et al. 2005; Kitagawa et al. 2006). Some other studies utilize fiber-reinforced self-compacting concrete, and composite structures like aluminum foam layers to mitigate the shock strength (Foglar et al. 2015; Hajek et al. 2016). Even though many studies have been done till now, practical devices are not yet available for shock wave mitigation and more efforts are still required in this field. Hence geometrical barriers were designed with almost zero obstruction area and implemented in this study. This strategy attenuates the shock wave significantly. Besides, it is a cost-effective, simple, and reliable method.

This study not only focuses on the analysis of shock wave propagation, reflection, and diffraction phenomenon in ducts but also on practical applications in engineering. Weak shock waves have various medical applications. The practical examples of strong shock waves are hazardous explosions in mining industries, an explosion in the military war field, gas transmission pipes, traumatic brain injury due to explosion/bomb blast, and other industrial explosions (Hicks et al. 2010; Sawyer et al. 2018). Followed by such explosions or accidents, the blast's effect was transmitted to very long distances as shock waves (Igra et al. 2013). The complex flow was created behind the shock front because of subsequent interactions between the transmitted shock wave and structures encountered by the shock. The shock wave in turn generates a highly unsteady flow. Hence in this study, the geometrical barrier was fixed in the flow field to mitigate the impulse of a propagating shock wave. Once the planar shock wave propagates and interacts with the geometrical barrier, the flow gets deflected continuously, and thereby the intensity of propagating shock is mitigated to an enormous extent.

In the present study, different geometric passages, zig-zag barriers, inclined barriers, and staggered vertical barriers were investigated for comparatively weak shock wave at shock Mach number $M_s = 3$. This strategy is the most simple and effective way to mitigate the shock wave compared to the existing methods. These barriers were designed with almost zero obstruction area. In the zig-zag barrier case, the barriers reflect and diffract the shock wave multiple times to mitigate the shock wave. In the inclined barrier case, the mitigation was achieved by diffusion of an initial shock wave which in turn increases the energy loss and mitigates the shock considerably. In a staggered vertical barrier case, the arrangement of a barrier in staggered form retards the mass motion velocity, and it results in a reduction of shock pressure significantly. The comparison of results shows that the maximum attenuation of 55.63% was achieved by the staggered vertical barrier case. Also, the numerical prediction by Navier Stokes and Euler equations is almost the same. Hence each method has significant advantages, and the numerical results show that the implementation of geometrical barriers has a considerable impact on the mitigation of shock wave.

2 Numerical analysis

2.1 Governing equations

In this study, the flow was modeled using Euler equations, which obey the ideal gas equation of state. It expresses the conservation of mass, momentum, and energy for inviscid compressible flow. The conservation equations were expressed as follows:

$$\frac{\partial}{\partial t}U + \frac{\partial}{\partial x}F(U) + \frac{\partial}{\partial y}G(U) = 0 \tag{1}$$

where

$$U = \begin{bmatrix} \rho \\ \rho u \\ \rho v \\ \rho E \end{bmatrix}. F(U) = \begin{bmatrix} \rho u \\ \rho u^2 + p \\ \rho uv \\ (\rho E + p)u \end{bmatrix}, G(U) = \begin{bmatrix} \rho v \\ \rho uv \\ \rho v^2 + p \\ (\rho E + p)v \end{bmatrix} \tag{2}$$

U is an unknown flow field variable vector, $F(U)$, and $G(U)$ are the flux terms in the x and y directions. P, E, u, v, and ρ are pressure, total specific energy, velocity components in x and y directions, and density.

The Navier–Stokes equations were used to find the conservation of mass, momentum, and energy along with the k-omega SST turbulence model was solved. The turbulence kinetic energy, k, and its rate of dissipation, ω, are obtained from the following equations as follows:

$$\frac{\partial}{\partial t}(\rho k) + \frac{\partial}{\partial x_i}(\rho k u_i) = \frac{\partial}{\partial x_j}\left[\Gamma_k \frac{\partial k}{\partial x_j}\right] + G_k - Y_k \tag{3}$$

and

$$\frac{\partial}{\partial t}(\rho \omega) + \frac{\partial}{\partial x_i}(\rho \omega u_i) = \frac{\partial}{\partial x_j}\left[\Gamma_\omega \frac{\partial \omega}{\partial x_j}\right] + G_\omega - Y_\omega + D_\omega \tag{4}$$

where G_k is the generations of turbulence kinetic energy due to the mean velocity gradients. $G\omega$ represents the generation of ω. Γ_k and $\Gamma\omega$ represent the effective diffusivity of K and ω, respectively. $D\omega$ represents the cross-diffusion term. Y_k and $Y\omega$ represent the dissipation of K and ω due to turbulence, respectively (Launder and Spalding 2013).

The ideal gas equation of state is given as follows:

$$p = (\gamma - 1)\rho e \tag{5}$$

where γ is the ratio of specific heat. e is the specific internal energy.

2.2 Computational flow field

The two-dimensional computational domain for different cases was shown in Fig. 1. The Shock tube consists of two chambers, the driver section (high-pressure chamber) and the driven section (low-pressure chamber). Both were designed with a length of 750 mm each and separated by a diaphragm. In this study, the driver pressure (P_4) and driven pressure (P_1) is 10.33 and 1 bar, respectively. When the diaphragm is ruptured, it simulates an initial plane shock front due to the pressure difference between the chambers. The shock front has very high acceleration, accompanied by pressure density and temperature jumps. In this study, to mitigate the shock wave in the driven section, three geometric barriers were designed and installed. Figure 1 shows that the different shock tube geometries were a) plain shock tube, b) zig-zag barrier (angle = 26.5°), c) inclined barrier (angle = 45°) d) staggered vertical barrier. Computational fluid dynamics (CFD) analysis has been carried out with different geometric barriers in the driven section. The geometric barrier in conventional cases has area blockage. The blockage ratio (BR) is defined as the ratio of the obstruction area of the shock tube (A_{obs}) to the initial shock tube area (A_o). In these geometric barriers, the area blockage is almost zero, and the mitigation of shock wave was achieved only through reflection and diffraction of shock waves.

2.3 Numerical scheme

Computational Fluid Dynamics (CFD) analyses were carried out to find the shock wave mitigation in the driven section of the shock tube. The commercial simulation package Ansys Fluent is employed. In this study, the inviscid and K-omega SST turbulence model is employed. The operating fluid used is air as an ideal gas. The unsteady Euler and Navier–Stokes equations were solved mathematically to get detailed flow physics. The driver (P_4) and driven (P_1) pressures are 10.33 and 1 bar, respectively. The second-order spatial

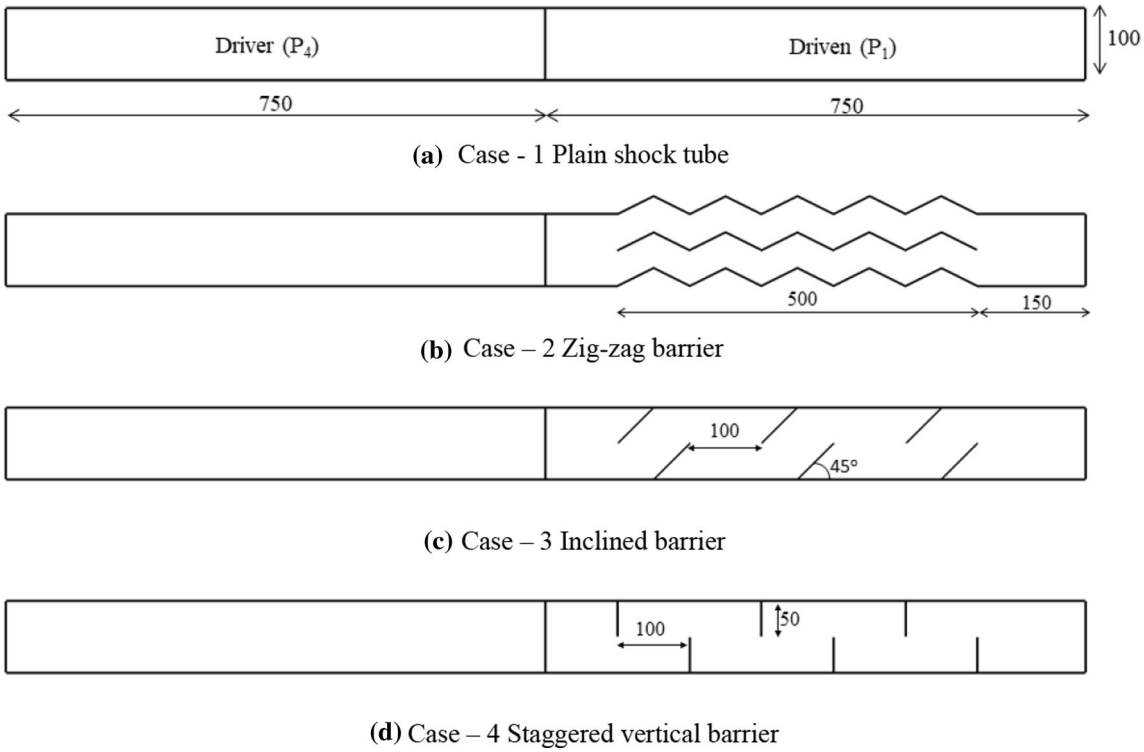

Fig. 1 Computational flow field of different shock mitigation designs (All dimensions are in mm)

discretization and transient formulation schemes were involved. The time step used for all the cases is 5e − 7 s. The smaller time step helps to capture the propagation and mitigation behavior of shock waves better. The CFL number was maintained at 0.5 and flux discretization used is Roe-FDS. The boundary condition of the shock tube and geometric passage is fixed as a wall.

2.4 Grid independence study

The grid plays a significant role in determining the flow field variables for a given problem. In this study, a structured grid is implemented, and commercial software Ansys ICEM CFD is used. The grid independence study for a plain shock tube case has been carried out with four different cases to predict the optimum grid size. The domain has been equally discretized using quadrilateral cells. Each case's total grid size is 0.42, 0.6, 0.94, and 1.67 million, and each grid corresponds to the physical length of 0.6 mm, 0.5 mm, 0.4 mm, and 0.3 mm, respectively. Figure 2 shows the static pressure along the centerline for different cases at time t = 1.2 ms. It clearly shows that the variation of static pressure between cases 3 and 4 is negligible. So, a further increase in grid size does not impact the results of flow field variables; it also increases the computation time. The result obtained from case 3 is independent of grid size for the plain shock tube. So for other cases, the mesh size of 0.4 mm is implemented.

3 Validation

The present CFD simulation is validated against the experiment work reported by Igra et al. In the experimental work, Igra et al. investigated the shock wave diffraction and mitigation of shock wave because of a large intermediate chamber placed inside the shock tube (Igra et al. 2001). The geometrical detail of the experimental setup is shown in Fig. 4b. The experimental and numerical results at different time frames were compared in Fig. 3. Figure 3a shows the initial shock just comes out of the shock tube. Figures 3b, c show the propagation of shock wave in a large intermediate chamber. Figure 3d shows the entry of the shock wave into the smaller section. All the shadowgraph images of numerical results match reasonably

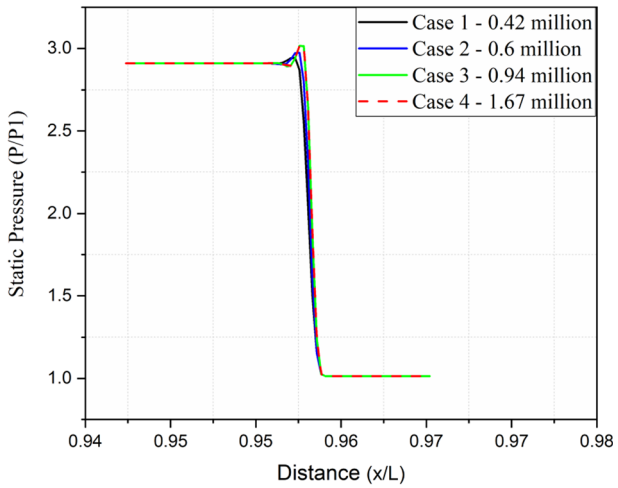

Fig. 2 Static pressure distributions along the centerline for the plain shock tube with different grids (t = 1.2 ms)

well with experimental results. The experimental work reported the pressure-time histories at different monitoring points.

The shock pressure jump at each monitoring point was extracted from the experimental results and validated against the corresponding CFD results. Figure 4a shows that the shock wave pressure of computational results matches reasonably well with experimental results at each monitoring point. As shown in Fig. 3, the shock reflection, shock diffraction, and other flow physics captured by the CFD model show good agreement with experimental results. Hence, this study's validation clearly shows that the present CFD model can predict shock reflection and diffraction patterns with reasonably good accuracy.

4 Results and discussion

4.1 Zig-zag barrier

Figure 5 shows the CFD results of the shock tube with the zig-zag barrier. The zig-zag barrier has three walls: upper wall, middle wall, and lower wall, as shown in Fig. 5a. After the rupture of the diaphragm, the shock wave propagates downstream. Once the shock front reaches the zig-zag barrier, the shock waves split by the zig-zag duct's middle wall. Now the transmitted shock wave (TSW) enters the zig-zag passage. The lower wall of the duct faces compression of shock waves, leading to shock reflection, as shown in Fig. 5a. Whereas the upper wall, undergoes the expansion of shock wave, resulting in shock wave diffraction. These effects were due to the duct geometry's deflection, as shown in Fig. 5a.

As shown in Fig. 5a, the zig-zag barrier's middle wall faces both shock diffraction and reflection, below and above the wall, respectively. As the shock wave propagates downstream, it forms three discontinuities like an incident wave, reflected wave, and mach stem at a single point, otherwise known as simple mach reflection (SMR) (Wu et al. 2019). Figure 5b shows the formation of a single mach reflection. A detailed monograph study by Ben-Dor describes different shock reflection patterns created by moving the shock front along with the wedges of different angles (Ben-Dor 1992). As the flow progresses further downstream, the reflected shock waves interact with each other and move upstream, which forms coalescence reflected shock waves (CRSW), as shown in Fig. 5e.

Now the shock wave enters the second deflection part of the zig-zag duct. The shock wave diffraction happens at the lower wall due to the expansion of shock waves, as shown in Fig. 5c. The shock wave reflection happens at the zig-zag duct's upper wall, as shown in Fig. 5c. As shown in Fig. 5d, the middle wall experiences a reversal in shock pattern in the second turn of the zig-zag duct. Hence the middle wall of the zig-zag duct faces shock reflection and diffraction below and above the wall, respectively. As the flow further downstream, the reflection of the shock wave from the top wall surface interacts with the reflected shock from the upper portion of the middle wall. Similarly, the shock wave's reflection from the lower

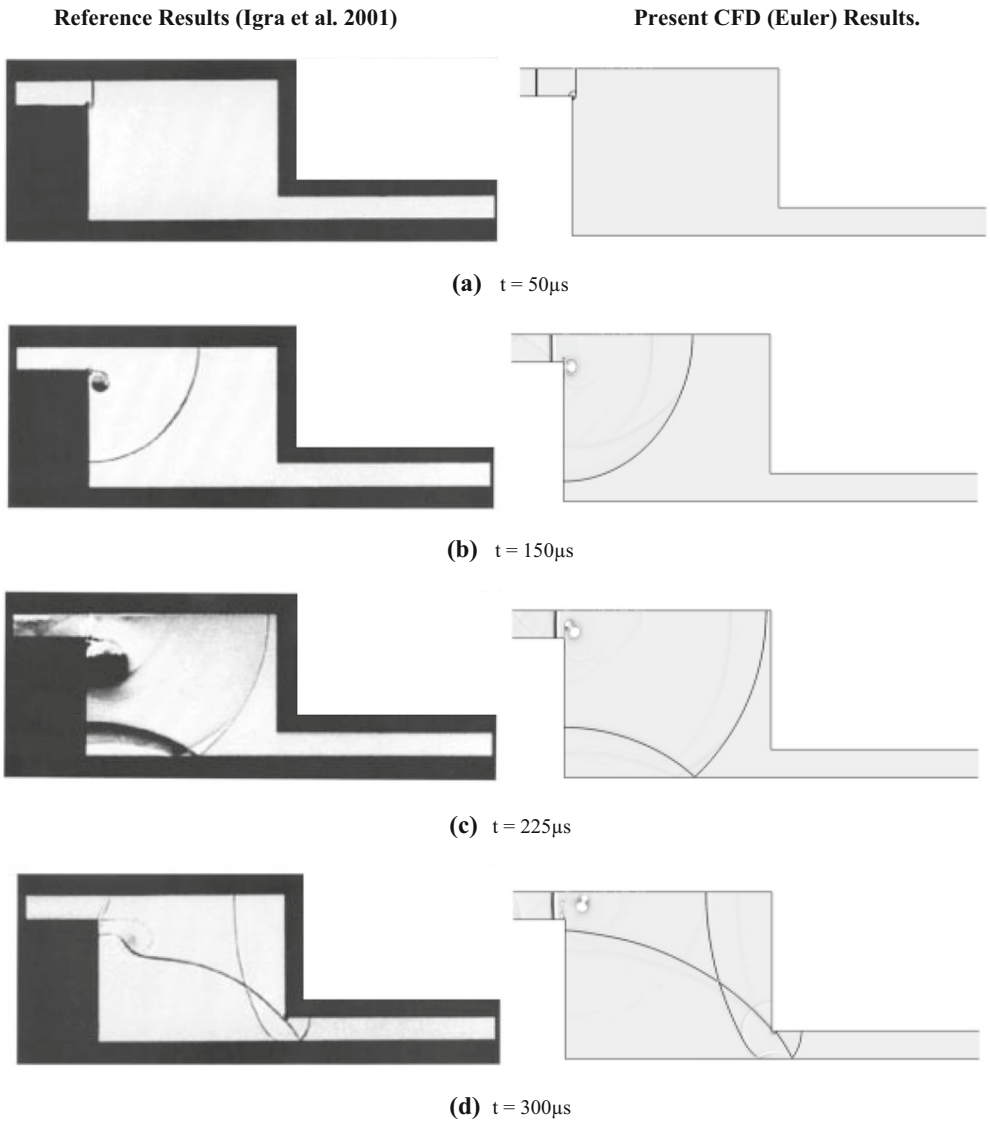

Fig. 3 Comparison of experimental (Ref. Igra et al. (2001) and numerical results at different time

portion of the middle wall interacts with a reflected shock wave from the bottom wall. This leads to multiple shock reflections, as shown in Fig. 5e.

This process is repeated as flow moves further downstream, which results in multiple shock reflections throughout the duct. Hence in this study, as the transmitted shock wave moves along the zig-zag passage, it undergoes shock wave reflection and diffraction consequently, as shown in Fig. 5a–e. As the shock front moves along the zig-zag passage, the shock pattern swaps from shock wave reflection to shock wave diffraction and vice versa. This cyclic and continuous interchanging of shock patterns results in the loss of shock strength. Hence in this study, the shock wave mitigation is achieved without much area obstruction along the flow path.

4.2 Inclined barrier

The CFD results of inclined barriers were shown in Fig. 6. As the flow approaches the first inclined barrier, it reflects the shock wave, and the other part transmits through the duct. The transmitted wave further diffracted from the lower portion of the first inclined barrier, as shown in Fig. 6a. As shown in Fig. 6b, the lower portion of the transmitted shock wave undergoes compression, and the shock wave gets reflected. As

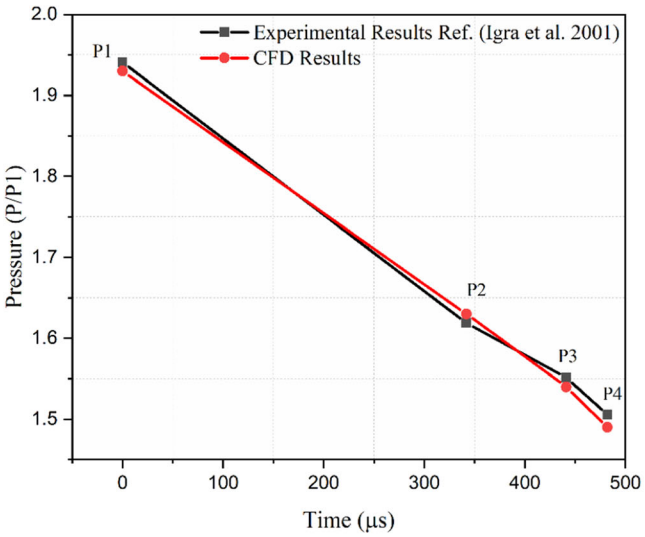

(a) Peak pressure comparison of Experimental and CFD results at different monitoring points (Ms=1.3466)

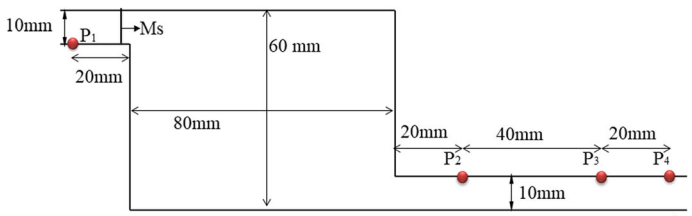

(b) Geometry of Experimental setup with monitoring points.

Fig. 4 **a** Peak pressure comparison of Experimental and CFD results at different monitoring points (M_s = 1.3466). **b** Geometry of Experimental setup with monitoring points

shown in Fig. 6c, when the shock wave propagates further downstream, it forms three discontinuities like an incident wave, reflected wave, and mach stem at a single point, which is otherwise known as simple mach reflection (SMR). As shown in Figs. 6a–e, these inclined barriers result in multiple shock wave reflections and interactions. These interactions increase the diffusion of an initial shock wave, which increases the energy loss of the shock. Also, the shock front will no longer be planar after crossing the geometric passage. The shock front losses the shock structure and shock strength due to inclined barriers. Hence the mitigation of shock wave is significantly higher.

4.3 Staggered vertical barrier

The CFD results of the staggered vertical barrier case were shown in Fig. 7. When the shock waves move over a staggered vertical barrier, it results in shock reflections. As the shock front impacts the barrier, part of the shock wave is reflected, and the rest of the flow is transmitted, as shown in Fig. 7a. As shown in Fig. 7b, The transmitted shock wave gets diffracted as it moves through the geometry corner. The diffracted waves move further downstream and reach the upper wall, which further reflects the shock wave, as shown in Fig. 7c. As shown in Fig. 7e, these multiple shock reflections increase the pressure locally in the flow field. The reflected shock wave merges and interacts with each other; it forms the coalescence reflected shock wave, which moves upstream, as shown in Fig. 7e. Moreover, the alternate flow obstruction due to the barrier retards the mass motion velocity, which results in the reduction of shock pressure. Hence in this study, the mitigation of shock wave is slightly higher compared to other cases.

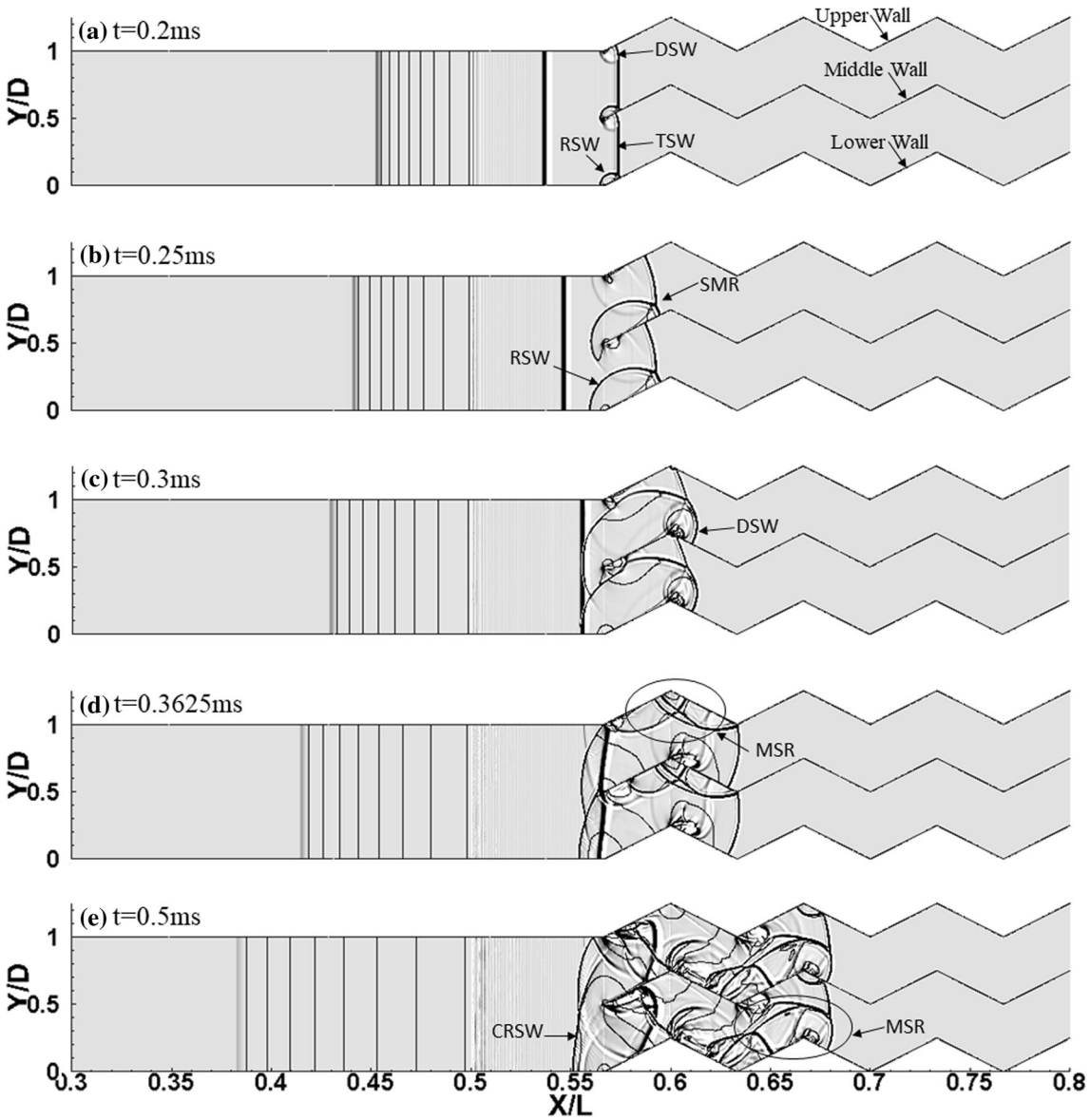

Fig. 5 Shock structures of Case-2 Zig-zag barrier at a different time (M_s = 3.0). TSW—Transmitted shock wave, RSW—Reflected shock wave, DSW—Diffracted shock wave, CRSW—Coalescence reflected shock wave, SMR—Simple Mach reflection, MSR—Multiple shock reflections

4.4 Navier Stokes simulation

In comparing all the cases, case 4 mitigates the shock wave better compared to other cases. Hence, in case 4, the Navier–Stokes model was employed to visualize the effect of viscosity, friction, heat transfer, and other effects on the mitigation of the shock wave. K-Omega SST model was involved in this study, and all other parameter remains the same as before. Figure 8 shows the simulation results of case 4 with the Navier–Stokes equations. The results of the Euler and Navier–Stokes simulation are almost the same with negligible differences.

The total simulation time is only 2.5 ms in such a small timeframe, heat transfer, and friction losses can be minimal compared to the incoming flow energy and momentum. So the boundary layer has minimal effects on the CFD results, as shown in Fig. 8. The transmitted shock waves undergo multiple reflections and diffraction patterns, which results in the mitigation of the shock wave, as shown in Fig. 8a–e. In this study, due to viscous and frictional effects, the shock wave mach number and shock strength were reduced

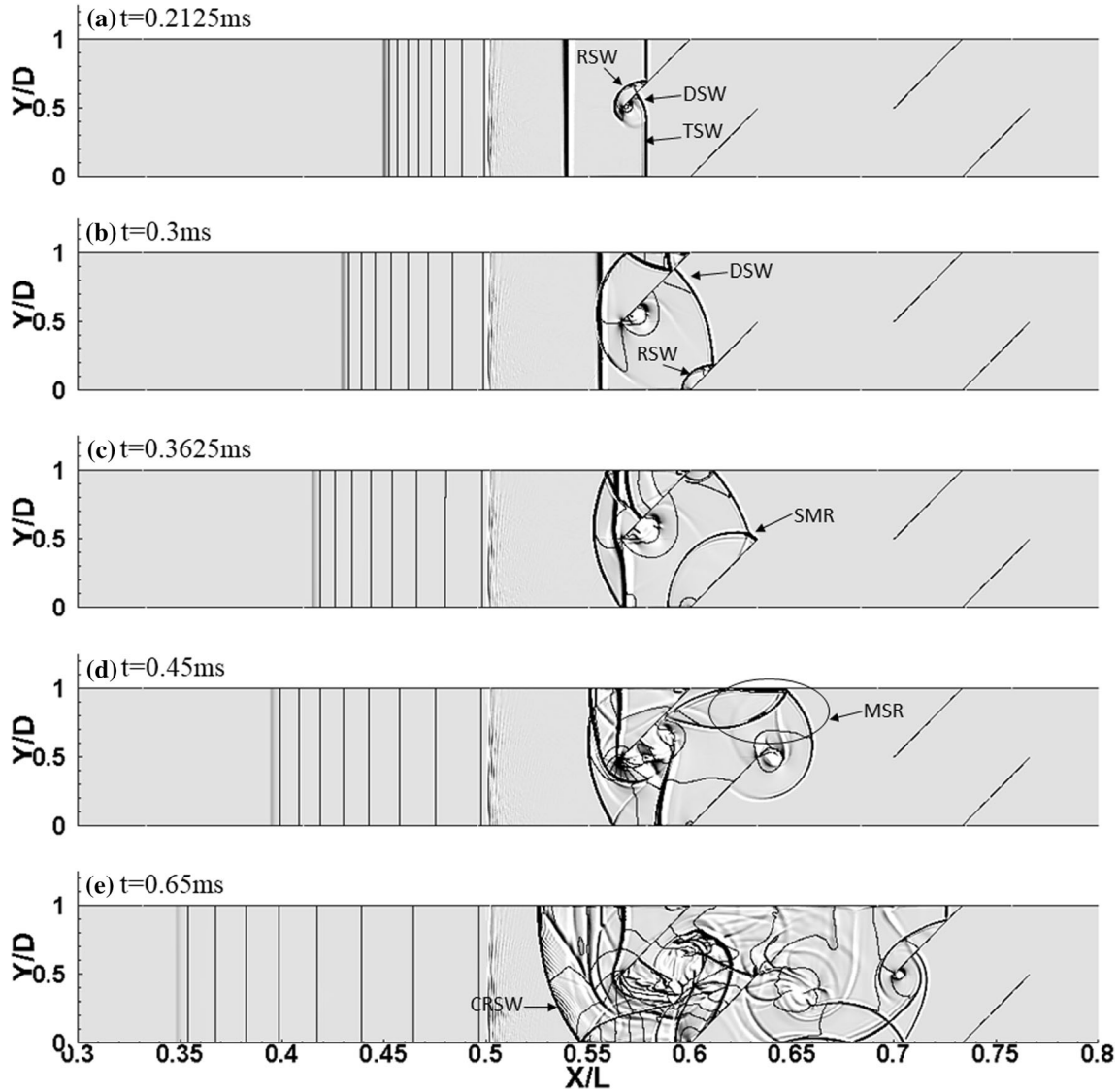

Fig. 6 Shock structures of Case-3 inclined barrier at a different time (M_s = 3.0)

slightly better compared to Euler simulation results. As shown in Fig. 9a, the pressure at the monitoring line shows that the shock front pressure predicted by Navier–Stokes and Euler equations is 1.354 bar and 1.356 bar, respectively. Hence it shows that the mitigation of shock wave predicted by the Navier–Stokes model and Euler model is almost the same.

4.5 Comparison of results

In this study, the shock wave's attenuation produced by different geometric barriers has been quantitatively measured at a monitoring line, as shown in Fig. 9. In this monitoring line, the mass-weighted average of static pressure jump along the shock front was measured and compared. Figure 9 shows the static pressure time histories for different cases at the monitoring line. The results clearly show that the shock wave mitigation is significant because of a geometric barrier compared to a plain shock tube. The maximum attenuation of the shock wave was observed in case 4 (N-S eqn) and case 4 (Euler), followed by case 3, and case 2, respectively. As shown in Fig. 9, the monitoring line can measure localized peak pressure. However, the attenuation by case 4 (N-S eqn & Euler) is so prominent in comparison with case 2 and case 3. This may be due to various factors like flow obstruction, multiple shock wave reflections, diffractions, etc.

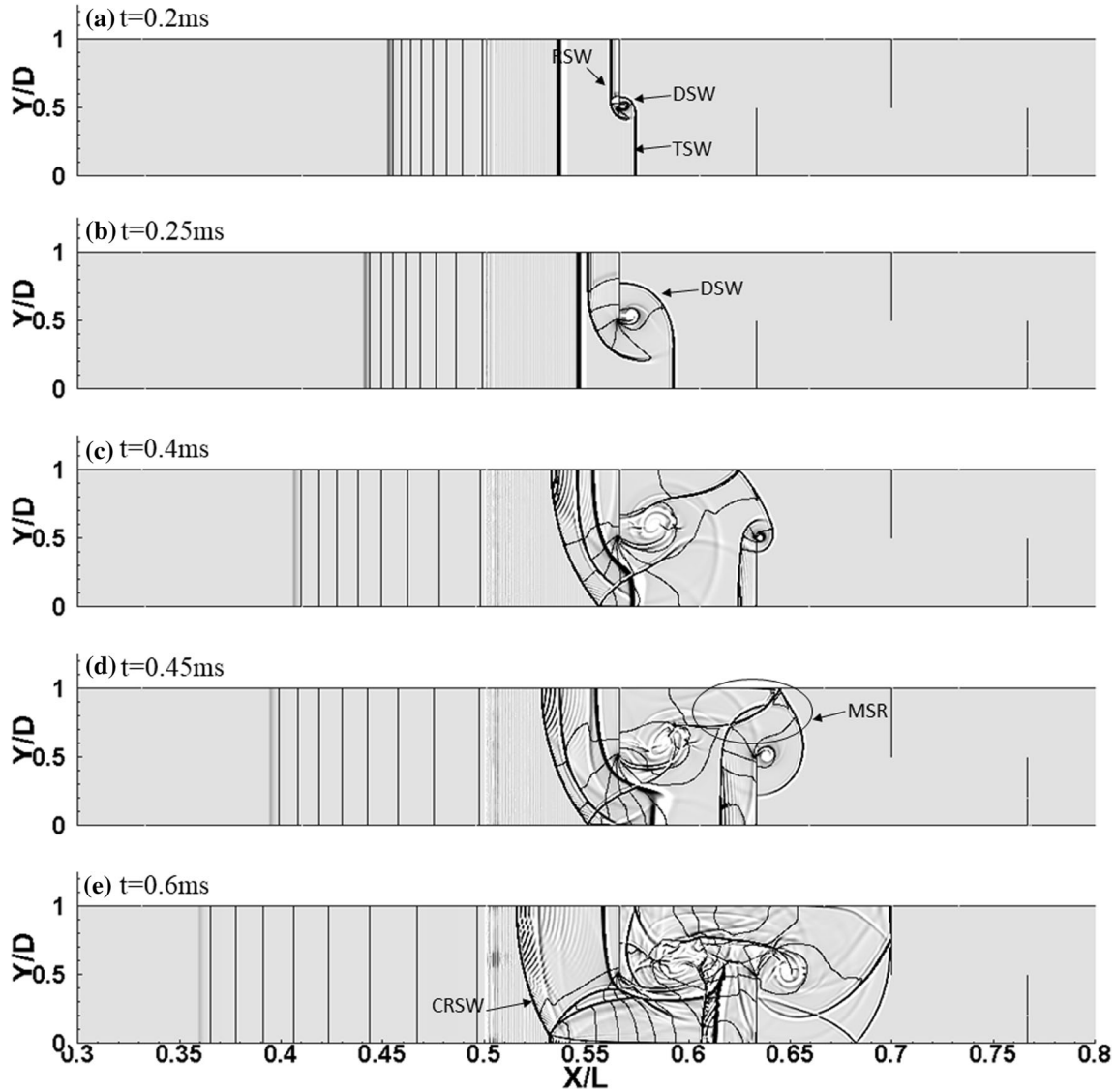

Fig. 7 Shock structures of Case-4 (Euler) staggered vertical barrier at a different time (M_s = 3.0)

The shock wave Mach number is another critical parameter to consider in the comparison of shock strength. The theoretical shock mach number (M_s) was calculated by

$$M_s = \sqrt{\frac{\gamma + 1}{2\gamma}\left(\frac{p_2}{p_1} - 1\right) + 1} \tag{6}$$

Figure 10 shows the shock wave mach number for different cases after crossing the geometric barriers. The shock wave was measured along with different time frames along the centerline in the downstream region. Figure 10 shows that the shock wave mach number was reduced significantly due to geometric barriers and energy dissipation due to multiple shock wave reflections and shock wave diffractions. By comparing different geometric passages, case 4 (N-S eqn & Euler) shows the noticeable reduction in shock wave mach number followed by case 3 and case 2, respectively.

$$\%\ \text{Reduction in shock pressure} = \frac{\text{Shock pressure at a monitoring line}}{\text{Shock pressure of plain shock tube at that monitoring line}} * 100 \tag{7}$$

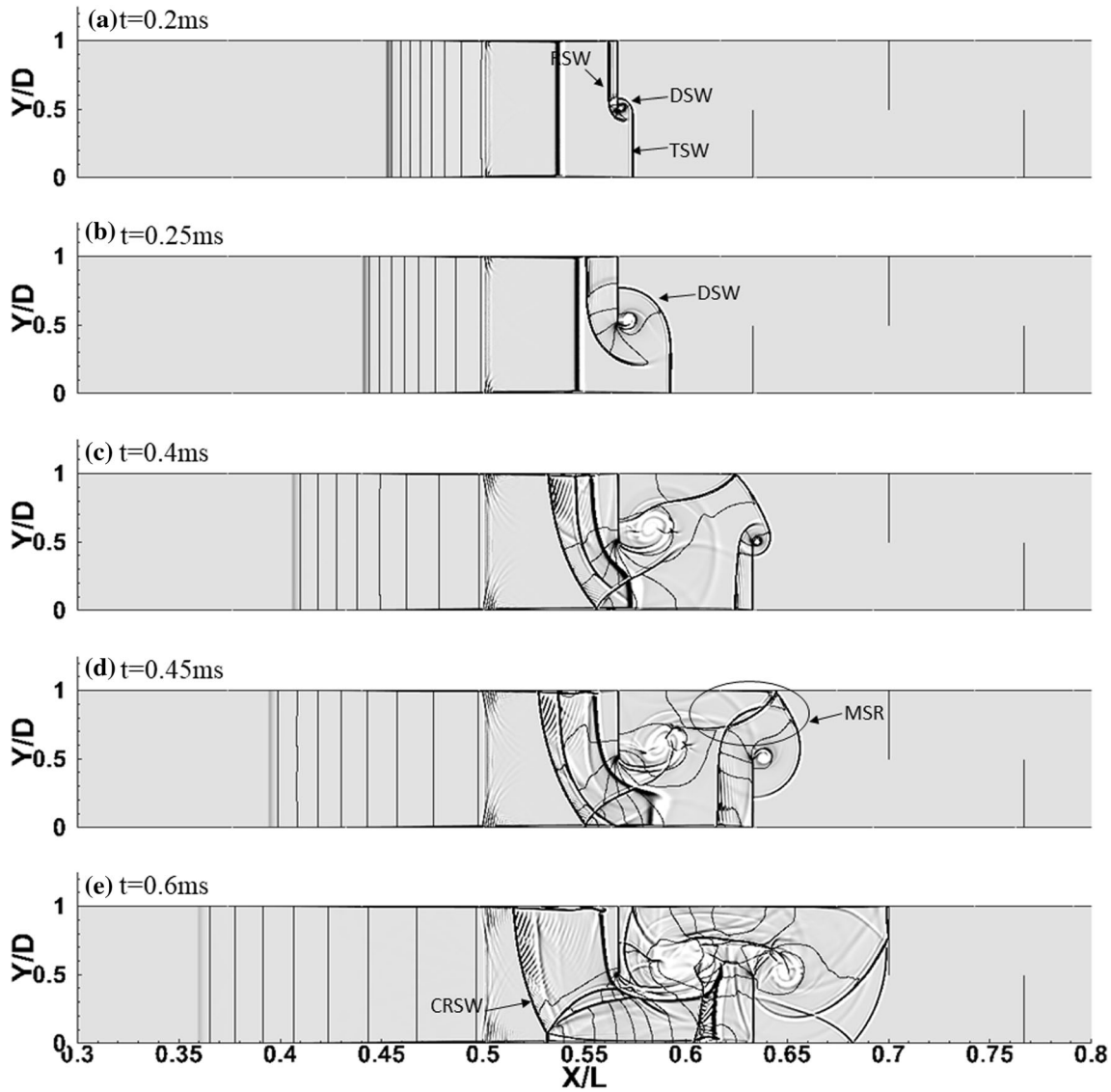

Fig. 8 Shock structures of Case-4 using Navier–Stokes model at a different time (M_s = 3.0)

Figure 11 shows the comparison of shock pressures of different geometric passages compared to plain shock tube at the monitoring line, as shown in Fig. 9. It shows the percentage reduction of shock pressure of 55.63% was obtained in case 4 (N-S eqn) followed by 55.57% in case 4 (Euler), 52.9% in case 3, and 19.4% in case 2 in comparison with plain shock tube at monitoring line.

Previous research on geometric barriers had shown that the effectiveness of shock mitigation increases with the obstruction area. But this work reports considerable shock mitigation with practically minimal obstruction area. Hence from these comparisons, it is evident that geometrical barriers significantly impact the mitigation of shock waves along the shock tube.

5 Conclusion

This study investigates the effectiveness of shock wave mitigation using different geometric barriers in the shock tube. In the validation study, the shock tube with a large intermediate chamber was designed, and numerical analysis was simulated. The computational fluid dynamics results of a large intermediate chamber

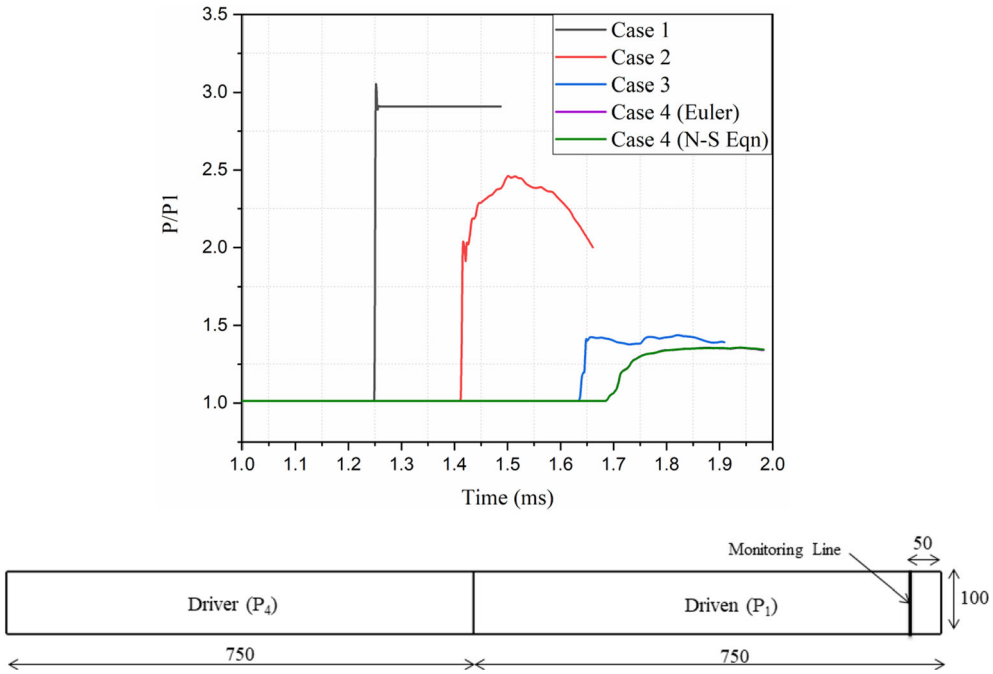

Fig. 9 Pressure time histories at monitoring line (P_4/P_1 = 10.33)

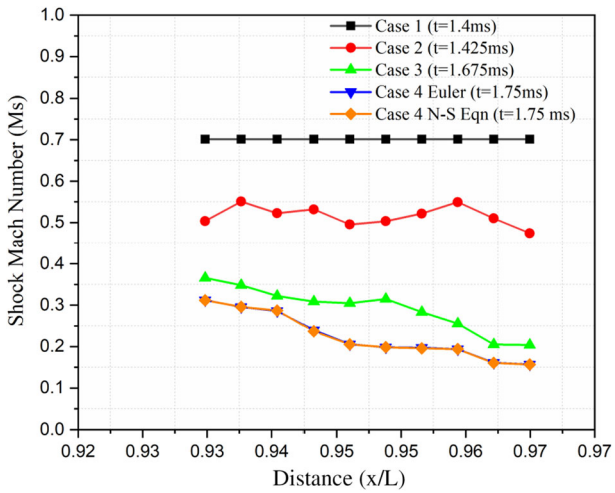

Fig. 10 Shock wave Mach number along the centerline for different cases

along the shock tube show good agreement with the previous experimental results. It shows that the model can predict the mitigation behavior of shock waves along the shock tube.

In the zig-zag barrier case, the shock front enters a geometrical passage and undergoes multiple shock reflection and diffraction due to compression and expansion, respectively, with very minimal obstruction area. In the inclined barrier case, the shock front undergoes multiple shock wave reflections and diffractions. These interactions increase the diffusion of the initial shock and reduce its strength considerably. As the shock strength was reduced due to inclined barriers the shock front lost its structure, and the shock wave was mitigated considerably.

In the staggered vertical barrier case, Navier Stokes and Euler model predict almost the same results. Because in such a small timeframe heat transfer, and friction losses can be minimal compared to the incoming flow energy and momentum. In this case, the alternate vertical barriers retard the mass motion velocity and mitigate the shock wave significantly. Hence on comparing the results, a maximum shock

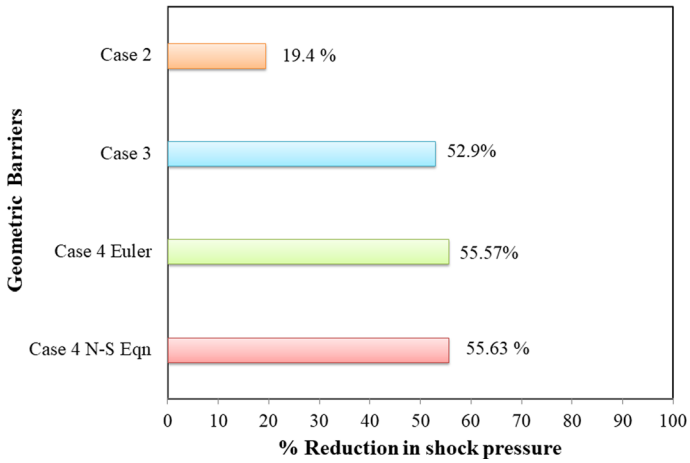

Fig. 11 Percentage reduction in shock pressure

attenuation of around 55.63% was achieved through this design. In all the cases, the shock front after crossing the geometric passage lost its shock strength significantly, and the shock structure was no more planar. Hence the implementation of geometrical barriers in the driven section of the shock tube plays a vital role in mitigating shock waves.

Acknowledgements This work was supported by the National Research Foundation of Korean (NRF) grant funded by the Korea government (MSIP) (No. NRF-2021R1I1A3044216).

References

Baer MR (1992) A numerical study of shock wave reflections on low density foam. Shock Waves 2:121–124. https://doi.org/10.1007/BF01415901

Bakken J, Slungaard T, Engebretsen T, Christensen SO (2003) Attenuation of shock waves by granular filters. Shock Waves 13:33–40. https://doi.org/10.1007/s00193-003-0180-7

Ben-Dor G (1992) Shock wave reflection phenomena. Shock Wave Reflect Phenom. https://doi.org/10.1007/978-1-4757-4279-4

Berger S, Sadot O, Ben-Dor G (2010) Experimental investigation on the shock-wave load attenuation by geometrical means. Shock Waves 20:29–40. https://doi.org/10.1007/s00193-009-0237-3

Britan A, Igra O, Ben-Dor G, Shapiro H (2006) Shock wave attenuation by grids and orifice plates. Shock Waves 16:1–15. https://doi.org/10.1007/s00193-006-0019-0

Britan A, Shapiro H, Liverts M et al (2013) Macro-mechanical modelling of blast wave mitigation in foams. Part I: review of available experiments and models. Shock Waves 23:5–23. https://doi.org/10.1007/s00193-012-0417-4

Chaudhuri A, Hadjadj A, Sadot O, Ben-Dor G (2013) Numerical study of shock-wave mitigation through matrices of solid obstacles. Shock Waves 23:91–101. https://doi.org/10.1007/s00193-012-0362-2

Foglar M, Hajek R, Kovar M, Štoller J (2015) Blast performance of RC panels with waste steel fibers. Constr Build Mater 94:536–546. https://doi.org/10.1016/j.conbuildmat.2015.07.082

Hajek R, Foglar M, Fladr J (2016) Influence of barrier material and barrier shape on blast wave mitigation. Constr Build Mater 120:54–64. https://doi.org/10.1016/j.conbuildmat.2016.05.078

Hicks RR, Fertig SJ, Desrocher RE et al (2010) Neurological effects of blast injury. J Trauma Inj Infect Crit Care 68:1257–1263. https://doi.org/10.1097/TA.0b013e3181d8956d

Igra O, Wu X, Falcovitz J et al (2001) Experimental and theoretical study of shock wave propagation through double-bend ducts. J Fluid Mech 437:255–282. https://doi.org/10.1017/S0022112001004098

Igra O, Falcovitz J, Houas L, Jourdan G (2013) Review of methods to attenuate shock/blast waves. Prog Aerosp Sci 58:1–35. https://doi.org/10.1016/j.paerosci.2012.08.003

Kitagawa K, Yasuhara M, Takayama K (2006) Attenuation of shock waves propagating in polyurethane foams. Shock Waves 15:437–445. https://doi.org/10.1007/s00193-006-0042-1

Launder and Spalding (2013) ANSYS, Inc, ANSYS Fluent User's Guide, Release 15.0. Canonsburg, PA 15317

Needham CE (2018) Blast waves, 2nd edn. Springer, Berlin, Heidelberg

Ohtomo F, Ohtani K, Takayama K (2005) Attenuation of shock waves propagating over arrayed baffle plates. Shock Waves 14:379–390. https://doi.org/10.1007/s00193-005-0282-5

Petel OE, Ouellet S, Higgins AJ, Frost DL (2013) The elastic-plastic behaviour of foam under shock loading. Shock Waves 23:55–67. https://doi.org/10.1007/s00193-012-0414-7

Rajasekar J, Kim TH, Kim HD (2020) Visualization of shock wave propagation due to underwater explosion. J vis. https://doi.org/10.1007/s12650-020-00664-9

Sawyer TW, Josey T, Wang Y et al (2018) Investigations of primary blast-induced traumatic brain injury. Shock Waves 28:85–99. https://doi.org/10.1007/s00193-017-0756-2
Sembian S, Liverts M, Apazidis N (2016) Attenuation of strong external blast by foam barriers. Phys Fluids. https://doi.org/10.1063/1.4963243
Sommerfeld M (1985) The unsteadiness of shock waves propagating through gas-particle mixtures. Exp Fluids 3:197–206. https://doi.org/10.1007/BF00265101
Song B, Chen WW, Dou S et al (2005) Strain-rate effects on elastic and early cell-collapse responses of a polystyrene foam. Int J Impact Eng 31:509–521. https://doi.org/10.1016/j.ijimpeng.2004.02.003
Sounik DF, Gansen P, Clemons JL, Liddle JW (1997) Head-impact testing of polyurethane energy-abosrbing (EA) foams. SAE Tech Pap. https://doi.org/10.4271/970160
Wu K, Zhang G, Kim HD (2019) Study on the Mach and regular reflections of shock wave. J vis 22:283–303. https://doi.org/10.1007/s12650-018-00542-5